Robust cardiac $T1_\rho$ mapping at 3T using adiabatic spin-lock preparations

Coletti, Chiara; Fotaki, Anastasia; Tourais, Joao; Zhao, Yidong; van de Steeg-Henzen, Christal; Akçakaya, Mehmet; Tao, Qian; Prieto, Claudia; Weingärtner, Sebastian

DOI
10.1002/mrm.29713

Publication date
2023

Document Version
Final published version

Published in
Magnetic Resonance in Medicine

Received: 5 August 2022 | Revised: 26 April 2023 | Accepted: 4 May 2023

DOI: 10.1002/mrm.29713

RESEARCH ARTICLE

Magnetic Resonance in Medicine

Robust cardiac $T_{1\rho}$ mapping at 3T using adiabatic spin-lock preparations

Chiara Coletti[1] | Anastasia Fotaki[2] | Joao Tourais[1] | Yidong Zhao[1] | Christal van de Steeg-Henzen[3] | Mehmet Akçakaya[4] | Qian Tao[1] | Claudia Prieto[2,5,6] | Sebastian Weingärtner[1]

[1]Department of Imaging Physics, Delft University of Technology, Delft, The Netherlands

[2]Department of Biomedical Engineering, King's College London, London, UK

[3]HollandPTC, Delft, The Netherlands

[4]Department of Electrical and Computer Engineering and Center for Magnetic Resonance Research, University of Minnesota, Minnesota Minneapolis, USA

[5]School of Engineering, Pontificia Universidad Católica de Chile, Santiago, Chile

[6]Milleniun Institute for Intelligent Healthcare Engineering iHEALTH, Santiago, Chile

Correspondence
Sebastian Weingärtner, Department of Imaging Physics, Delft University of Technology, Lorentzweg 1, 2628 CJ, Delft, The Netherlands.
Email: s.weingartner@tudelft.nl

Funding information
4TU Precision Medicine program supported by High Tech for a Sustainable Future, a framework commissioned by the four Universities of Technology of the Netherlands; Nederlandse Organisatie voor Wetenschappelijk Onderzoek (NWO) Start-up Grant, Grant/Award Number: STU.019.024; ZonMw Off-Road, Grant/Award Number: 04510011910073; ANID - Millennium Science Initiative Program, Grant/Award Number: ICN2021_004; National Institute of Health (NIH), Grant/Award Numbers: R21EB028369, R01HL153146, P41EB027061

Purpose: The aim of this study is to develop and optimize an adiabatic $T_{1\rho}$ ($T_{1\rho,adiab}$) mapping method for robust quantification of spin-lock (SL) relaxation in the myocardium at 3T.

Methods: Adiabatic SL (aSL) preparations were optimized for resilience against B_0 and B_1^+ inhomogeneities using Bloch simulations. Optimized B_0-aSL, Bal-aSL and B_1-aSL modules, each compensating for different inhomogeneities, were first validated in phantom and human calf. Myocardial $T_{1\rho}$ mapping was performed using a single breath-hold cardiac-triggered bSSFP-based sequence. Then, optimized $T_{1\rho,adiab}$ preparations were compared to each other and to conventional SL-prepared $T_{1\rho}$ maps (RefSL) in phantoms to assess repeatability, and in 13 healthy subjects to investigate image quality, precision, reproducibility and intersubject variability. Finally, aSL and RefSL sequences were tested on six patients with known or suspected cardiovascular disease and compared with LGE, T_1, and ECV mapping.

Results: The highest $T_{1\rho,adiab}$ preparation efficiency was obtained in simulations for modules comprising 2 HS pulses of 30 ms each. In vivo $T_{1\rho,adiab}$ maps yielded significantly higher quality than RefSL maps. Average myocardial $T_{1\rho,adiab}$ values were 183.28 ± 25.53 ms, compared with 38.21 ± 14.37 ms RefSL-prepared $T_{1\rho}$. $T_{1\rho,adiab}$ maps showed a significant improvement in precision (avg. 14.47 ± 3.71% aSL, 37.61 ± 19.42% RefSL, $p < 0.01$) and reproducibility (avg. 4.64 ± 2.18% aSL, 47.39 ± 12.06% RefSL, $p < 0.0001$), with decreased inter-subject variability (avg. 8.76 ± 3.65% aSL, 51.90 ± 15.27% RefSL, $p < 0.0001$). Among aSL preparations, B_0-aSL achieved the better inter-subject variability. In patients, B_1-aSL preparations showed the best artifact resilience among the adiabatic preparations. $T_{1\rho,adiab}$ times show focal alteration colocalized with areas of hyper-enhancement in the LGE images.

Conclusion: Adiabatic preparations enable robust in vivo quantification of myocardial SL relaxation times at 3T.

KEYWORDS
adiabatic RF, B_0/B_1^+ inhomogeneities, myocardium, spin-lock relaxation, $T_{1\rho}$ mapping

1 | INTRODUCTION

Cardiac MRI is the clinical gold standard for the assessment of scar and fibrosis in ischemic and nonischemic heart diseases.[1-4] Late gadolinium enhancement (LGE) imaging can be used to differentiate between scar and healthy myocardium based on the retention of gadolinium-based contrast agents.[5] However, gadolinium-based contrast agent injection is contraindicated in patients with severe renal impairment due to the risk of necrotic systemic fibrosis.[6] In addition, gadolinium retention in the brain after injection of gadolinium-based contrast agents has been reported.[7] Thus, contrast-free alternatives are highly desired.

Quantitative myocardial tissue characterization has emerged with a wide spectrum of applications in various cardiomyopathies.[8] Native T_1 mapping has been explored for the assessment of myocardial infarction (MI) without the need for contrast agents.[9-11] However, mixed results have been reported on its sensitivity to focal scar and the approach remains the subject of ongoing research.[12-14]

$T_{1\rho}$ mapping has been proposed as a promising non-contrast alternative for scar assessment, due to its increased sensitivity to slow molecular motion in the kilohertz range.[15,16] First, Muthupillai et al. reported stronger postcontrast enhancement in acute MI cases for $T_{1\rho}$-weighted imaging compared with conventional T_1-weighted LGE imaging.[17,18] More recently, quantitative $T_{1\rho}$ maps have demonstrated improved differentiation between infarcted and remote myocardium in swine models, compared with native T_1 and T_2 maps, yielding comparable contrast-to-noise ratio (CNR) to LGE images.[13,19,20] Similar results have been reported in mice[21-23] and monkeys.[24] In vivo $T_{1\rho}$ mapping has been successfully applied in patients with ischemic and nonischemic cardiomyopathies at 1.5T.[25-30] Implementing $T_{1\rho}$ mapping at 3T could further improve the diagnostic value of this approach, due to an increase in signal-to-noise ratio and CNR, and the applicability in a growing number of 3T cardiac examinations. However, at 3T, only a few studies have been reported,[31-33] highlighting limitations related to system imperfections and the specific absorption rate (SAR) at high field strengths.

Conventional $T_{1\rho}$ maps are obtained using spin-lock (SL) preparation pulses with various durations, which are most commonly based on continuous-wave radiofrequency (RF) irradiation. These preparations are inherently susceptible to B_0 and B_1^+ field inhomogeneities.[34,35] To compensate for these inhomogeneities, continuous-wave SL pulses, in combination with refocusing pulses and phase cycling of SL modules, have been proposed.[34,36,37]

An alternative strategy to achieve resilience against system imperfections is the use of adiabatic pulses.[38] The robustness of adiabatic pulses against field inhomogeneities has been studied in other 3T cardiac MRI methods, such as inversion-recovery T_1 mapping[39] or refocusing in T_2 preparations.[40] Recently, similar adiabatic pulses have also been employed for refocusing in conventional SL preparations for cardiac $T_{1\rho}$ mapping[29] at 1.5T. Alternatively, SL preparations consisting of trains of adiabatic full passage pulses have been proposed to generate $T_{1\rho}$ contrast in other anatomies.[41,42] During the adiabatic full passage frequency sweep, the magnetization is locked along the effective field. This induces $T_{1\rho,\mathrm{adiab}}$ as the dominant relaxation mechanism during the pulse application.[43,44] $T_{1\rho,\mathrm{adiab}}$ will be used throughout the manuscript to indicate the rotating frame of reference relaxation constant measured by adiabatic preparations.

In this work, we sought to investigate the use of fully adiabatic SL (aSL) preparations for $T_{1\rho,\mathrm{adiab}}$ mapping of the myocardium at 3T. Bloch simulations were performed to optimize aSL pulse shapes for resilience against system imperfections. Phantom and in vivo imaging of the calf muscle were then carried out to compare aSL preparations against fully compensated conventional SL preparations. In vivo performance was shown with cardiac mapping in healthy subjects. Finally, clinical feasibility was evaluated in a small proof-of-principle cohort of patients.

2 | METHODS

2.1 | Adiabatic SL preparation design

In this work, aSL preparations were based on a train of adiabatic full passage pulses with an identical duration (Figure 1B). An even number of pulses was used to ensure that, at the end of the preparation ($t = \tau_{\mathrm{SL}}$), the magnetization $M(\tau_{\mathrm{SL}})$ was stored along the $+z$ direction. Hyperbolic secant (HS) pulse shapes were employed, as commonly used in other imaging applications.[39-41,45,46] These are characterized by the following amplitude and frequency modulation functions:

$$B_1(t) = B_1^{\max} \cdot \mathrm{sech}\left(\beta\left(\frac{2t}{\tau_{\mathrm{HS}}} - 1\right)\right), \quad (1)$$

$$\Delta\omega_1(t) = \omega_1(t) - \omega_0 = 2f_{\max} \cdot \tanh\left(\beta\left(\frac{2t}{\tau_{\mathrm{HS}}} - 1\right)\right). \quad (2)$$

Here $B_1(t)$ represents the pulse amplitude, $B_1^{\max}$ the peak amplitude, and β a constant that characterizes the width of the pulse bell. The single HS pulse duration is indicated by τ_{HS}. $\Delta\omega_1(t) = d\Phi_1(t)/\,dt$ is the frequency modulation with respect to the Larmor frequency ω_0, where $\Phi_1(t)$ represents the pulse phase as a function of time,

and $2f_{max}$ is the amplitude of the frequency sweep. The polarity of the frequency sweep was alternated between consecutive HS pulses to compensate for residual pulse imperfections.

Preparations with variable SL durations were achieved by concatenating identical pulse modules multiple times. The total duration of a single aSL module (τ_{SL}) was fixed to 60 ms. This value was chosen as a trade-off between adequate sampling of the expected range of in vivo $T_{1\rho,adiab}$ times and restrictions imposed by the SAR limits (whole-body SAR <2.0 W/kg) and the RF amplifier chain. To obtain constant preparation times when changing the pulse duration (τ_{HS}), modules containing 2, 4, or 8 HS pulses (2HS-aSL, 4HS-aSL, and 8HS-aSL) with relative pulse duration $\tau_{SL}/2$, $\tau_{SL}/4$, and $\tau_{SL}/8$, were implemented. For SL modules with 4 and 8 HS pulses, phase cycling was adopted between pairs of HS pulses to achieve a full Malcolm–Levitt (MLEV) scheme compensation.[47]

2.1.1 | Bloch simulations

Bloch simulations were used to optimize β, f_{max}, and τ_{HS} in the aSL preparations. All simulations were performed in MATLAB (MathWorks).

The preparation efficiency was determined as $M_z(\tau_{SL})/M(0)$ and used as a metric to optimize the design of the aSL module. The aSL preparation modules were simulated using the maximum RF pulse power, within the limits imposed by the peak B_1^+ (B_1^{max} = 13.5 μT) and SAR (whole-body SAR <2.0 W/kg). The preparation efficiency was averaged over a design window covering the expected range of in vivo off-resonances ($\Delta\omega_1^{off} \in \{-150, -149, ... + 150\}$ Hz) and B_1^+ inhomogeneities ($\zeta_1 \in \{0.50, 0.49, ...1.00\}$),[48-50] where ζ_1 indicates the ratio between the effective and nominal B_1^+ power.

Two sets of optimizations were performed to identify the optimal pulse duration and amplitude/frequency modulation functions, respectively. First, the 2HS-aSL, 4HS-aSL, and 8HS-aSL modules were compared in terms of preparation efficiency. Then, the module that produced the highest preparation efficiency was selected to derive the optimal values of β and f_{max}. Bloch simulations covering the range of expected in vivo variability of B_0 and B_1^+ were performed to obtain optimized pulses for three design regions: (1) original balanced design region (Bal-aSL) ($\Delta\omega_1^{off} \in \{-150, -149, ... + 150\}$ Hz, $\zeta_1 \in \{0.50, 0.49, ...1.00\}$); (2) B_0-skewed (B_0-aSL) ($\Delta\omega_1^{off} \in \{-200, -199, ... + 200\}$ Hz, $\zeta_1 \in \{0.75, 0.76, ...1.00\}$); 3) B_1^+-skewed design regions (B_1-aSL) ($\Delta\omega_1^{off} \in \{-100, -99, ... + 100\}$ Hz, $\zeta_1 \in \{0.25, 0.26, ...1.00\}$).

2.1.2 | Pulse design validation

Phantom data were acquired to validate the simulation results. The preparation efficiency of three optimized SL modules B_0-aSL, Bal-aSL, and B_1-aSL was tested on the phantom by modifying the center frequency $\Delta\omega_1^{off} \in \{-200, -180, ... + 200\}$ Hz and scaling the pulse power by $\zeta_1 \in \{0.1, 0.2, ...1.0\}$. A single-bottle phantom (Spectrasyn 4 polyalphaolefin, ExxonMobil Chemical) was used for the experiments.

The same experiments were performed in vivo in the calf muscle of a healthy subject (21 years old) to validate simulations and phantom experiments for the three aSL preparations. Here, B_0 and B_1^+ inhomogeneities were varied in fewer steps ($\Delta\omega_1^{off} \in \{-200, -150, ... + 200\}$ Hz, $\zeta_1 \in \{0.2, 0.4, ...1.0\}$).

For each SL module, $\Delta\omega_1^{off}$ and ζ_1, two snap-shot balanced steady-state free-precession (bSSFP) images were acquired: one preceded by the aSL preparation (τ_{SL} = 60ms) and one with no preparation. The two scans were interleaved by a 5-s pause to allow longitudinal magnetization recovery. Low imaging resolution was used ($10 \times 10 \times 10\ mm^3$), with pulse repetition time = 1.9 ms, echo time = 0.72 ms, flip angle = 90° and a SENSE factor of 2. The preparation efficiency $M_z(\tau_{SL})/M(0)$ was then calculated as the ratio of the two magnitude images. Signal polarity was restored using the corresponding phase images prior to further processing. In phantoms, the entire phantom area was evaluated, while in the calf, manually drawn circular regions of interest (ROIs) were used.

2.2 | $T_{1\rho}$ mapping

The proposed $T_{1\rho,adiab}$ mapping approaches were compared to each other and to a conventional, continuous-wave $T_{1\rho}$ mapping implementation in phantom and through in vivo experiments in the calf muscle and in the myocardium for healthy subjects and patients. Phantoms and healthy subjects were scanned on a 3T Ingenia system (Philips). Patient data were acquired on a 3T Achieva system (Philips). In vivo imaging was ethically approved by the competent review authorities (METC NL73381.078.20, UK National Research Ethics Service 15/NS/0030). Written informed consent has been obtained prior to all imaging sessions according to institutional guidelines.

The aSL preparations were compared to a fully balanced non-aSL pulse[37] (RefSL in Figure 1A). Three phase-cycled SL blocks with equal amplitude and durations of $\tau_{SL}/4$, $\tau_{SL}/2$, and $\tau_{SL}/4$, respectively, were played. The SL amplitude was chosen based on the RF amplifier constraints as $B_1^+/\gamma = 300$ Hz.

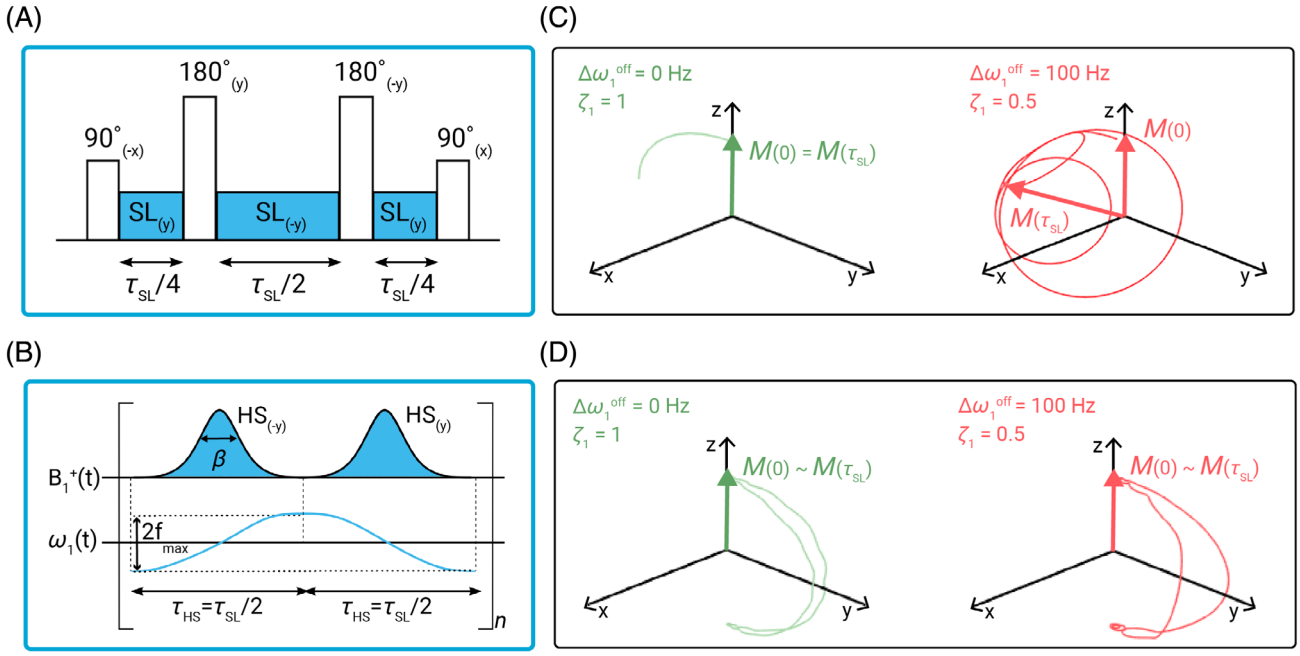

FIGURE 1 (A) Conventional spin-lock (SL) pulse (RefSL) and (B) adiabatic SL pulse (aSL), with corresponding amplitude and frequency modulation functions. Magnetization trajectories for the RefSL (C) and aSL (D) modules, simulated under ideal conditions (off-resonance $\Delta\omega_1^{off} = 0$ Hz, relative B_1^+ $\zeta_1 = 1$) and in presence of moderate B_0 and B_1^+ inhomogeneities ($\Delta\omega_1^{off} = 100$ Hz, $\zeta_1 = 0.5$). The parameters used for aSL were: $\tau_{HS} = 30$ms, $\beta = 5.5$, $f_{max} = 350$ Hz, $B_1^{max} = 13.5$ μT. Major deviations from the idealized case are observed for the RefSL preparation in the presence of inhomogeneities, while the aSL preparation produces similar results in both cases.

$T_{1\rho}$ and $T_{1\rho,adiab}$ mapping was performed using a cardiac triggered breath-hold sequence (Figure 2). Five baseline single-shot bSSFP images were acquired: the first with no SL preparation, then three with increasing SL durations, and finally a saturation-prepared image used to approximate infinite SL length.[51] A composite "Water suppression Enhanced through T1-effects" pulse was used to achieve robust saturation in the presence of field inhomogeneities.[52] Total preparation durations were τ_{SL} = 0, 60, 120, 180 ms for aSL modules. Shorter preparations were employed for RefSL (τ_{SL} = 0, 12, 24, 36 ms) to account for higher SAR levels, heavier RF amplifier load, and significantly shorter nonadiabatic $T_{1\rho}$ times. Scans were acquired in the end-diastolic phase. All images, except the saturation-prepared image, were preceded by a pause to allow for longitudinal magnetization recovery. Other imaging parameters were: in-plane resolution = 2 × 2 mm^2, field of view = 220 × 220 mm^2, slice thickness = 8 mm, echo time/pulse repetition time = 1.2/2.4 ms, flip angle = 70°, SENSE = 2.

$T_{1\rho}$ and $T_{1\rho,adiab}$ maps were reconstructed in MATLAB using the following three-parameter model,[51] to account for the effect of the imaging pulses:

$$S(t) = A \cdot e^{-\frac{t}{T_{1\rho(,adiab)}}} + B. \quad (3)$$

2.2.1 | Phantom and in vivo calf experiments

The T1MES phantom was used for phantom experiments to mimic blood and myocardium relaxation times at 3T.[53] Approximate T_1 and T_2 times of the phantom vials were estimated, using a MOLLI sequence for T_1 and a Gradient Spin Echo sequence for T_2. To study repeatability, ten repetitions of $T_{1\rho}$ and $T_{1\rho,adiab}$ mapping scans were acquired for each preparation (B_0-aSL, Bal-aSL, B_1-aSL and RefSL). Manually drawn circular ROIs were used to extract $T_{1\rho}$ and $T_{1\rho,adiab}$ values for further processing. Repeatability was assessed using the coefficient of variability ($\overline{CV}$):

$$\overline{CV} = \sum_{i=1}^{N_v} \frac{\overline{wCV_i}}{N_v}, \quad (4)$$

where N_v is the number of samples, corresponding to the number of vials in this case, and $\overline{wCV_i}$ is the coefficient of variability within the sample computed for every vial as

$$\overline{wCV_i} = \frac{1}{R}\sum_{r=1}^{R} \frac{\sqrt{(\mu_{i,r} - \overline{\mu_i})^2}}{\overline{\mu_i}}. \quad (5)$$

Here, R = 10 represents the number of repetitions, $\mu_{i,r}$ is the average $T_{1\rho}$ or $T_{1\rho,adiab}$ value for each vial i and

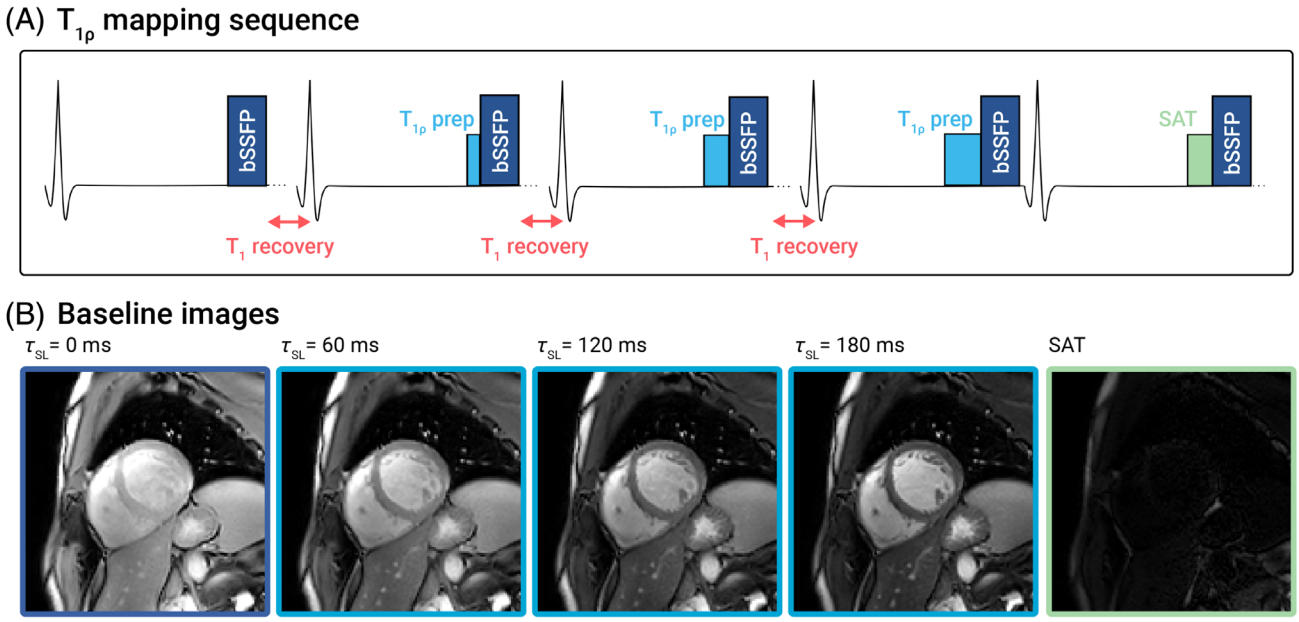

FIGURE 2 (A) $T_{1\rho}$ mapping sequence diagram with (B) corresponding baseline images from a representative healthy subject. Five images are acquired, one without preparation, three with different $T_{1\rho,adiab}$ preparations (τ_{SL} = 60, 120, 180ms), and one with saturation preparation, to allow for accurate mapping of the induced $T_{1\rho}$ relaxation.

repetition r and $\overline{\mu_i}$ is the average $T_{1\rho}$ or $T_{1\rho,adiab}$ value for each vial across all repetitions.

In a second experiment, $T_{1\rho,adiab}$ time was assessed as a function of the HS shape parameter β by acquiring phantom and calf $T_{1\rho,adiab}$ maps for $\beta \in 1, 2, \ldots 10$. For each β, a constant sweep amplitude f_{max} value was acquired. The dependence between the parameter β and the measured $T_{1\rho,adiab}$ values was tested using linear regression. R^2 coefficient, slope, and intercept values were reported for a single exemplary vial and a manually drawn circular calf ROI.

2.2.2 | Healthy subjects experiments

The proposed aSL preparations were tested in six healthy subjects (four males, two females, 21.5 ± 1.9 years old). For each subject, B_0-aSL, Bal-aSL, and B_1-aSL $T_{1\rho,adiab}$ maps were acquired in three short-axis (SAX) slices (basal, mid, and apical) and a four-chamber view. To assess reproducibility, the 12 maps were re-acquired following the repositioning of the subject.[54] In this cohort of healthy subjects, the magnetization recovery pause was 2.5 s to limit the total scan time to 13 s.

In a second cohort of seven healthy subjects (five males, two females, 24.7 ± 2.5 years old), the best-performing aSL preparation was compared to RefSL. Similarly to the first cohort, three SAX slices and a four-chamber view were acquired for each subject and preparation. Here, a magnetization recovery pause of 3.5 s was employed to avoid relaxation time over-estimation (see Figure S1). To assess robustness to B_0 and B_1^+ inhomogeneities, a second repetition of each map was acquired by moving the shimming volume only on the right ventricle, while keeping the position of the patient fixed.

The myocardium was automatically segmented using the nnU-Net framework[55] with uncertainty estimation.[56] Segmentation maps with predictive confidence below 75% were discarded and the segmentation was performed manually. The average values of $T_{1\rho}$ or $T_{1\rho,adiab}$ and their corresponding SD values (SD) in the segmented myocardium were extracted according to the American Heart Association (AHA) 16 segment model. A group-wise ANOVA test followed by paired t-tests was used to assess statistical differences between the $T_{1\rho}$ and $T_{1\rho,adiab}$ times with different preparations.

$T_{1\rho}$ and $T_{1\rho,adiab}$ quantification precision was assessed for each myocardial segment and SL module through the within-subject coefficient of variability (wCV):

$$\mathrm{wCV}_{r,i} = \frac{\sqrt{\sigma_{r,i}^2}}{\mu_{r,i}}, \tag{6}$$

computed for every repetition r and subject i, where μ and σ are the $T_{1\rho}$ or $T_{1\rho,adiab}$ mean and SD, respectively. Then, the mean and SD of $T_{1\rho}$ or $T_{1\rho,adiab}$ values across repetitions were computed as:

$$\overline{\mu}_i = \sum_{r=1}^{R} \frac{\mu_{r,i}}{R}, \overline{\sigma}_i = \frac{1}{R}\sqrt{\sum_{r=1}^{R}(\mu_{r,i} - \overline{\mu}_i)^2}, \tag{7}$$

and, therefore, the reproducibility as:

$$\overline{\mathrm{wCV}}_i = \bar{\sigma}_i/\bar{\mu}_i, \tag{8}$$

where $R = 2$ indicates the number of repetitions. Finally, the inter-subject variability was computed as a summary of the deviation of each subject's average $T_{1\rho}$ or $T_{1\rho,\mathrm{adiab}}$ value from the overall mean:

$$\overline{\mathrm{CV}} = \bar{\bar{\sigma}}/\bar{\bar{\mu}}, \tag{9}$$

where

$$\bar{\bar{\mu}} = \sum_{i=1}^{N} \frac{\bar{\mu}}{N_s}, \bar{\bar{\sigma}} = \frac{1}{N_s}\sqrt{\sum_{i=1}^{N_s}(\bar{\mu}_i - \bar{\bar{\mu}})^2}, \tag{10}$$

and N_s indicates the number of subjects. Statistical differences between the different SL preparations in terms of precision and reproducibility were investigated using a group-wise Kruskal–Wallis test and subsequently right-tailed pair-wise Mann–Whitney U-tests.

2.2.3 | Patients experiments

Clinical feasibility was tested in a small proof-of-principle cohort of six patients (two males, four females, 50.2 ± 11.0 years old) referred to clinical CMR. All patients were imaged using standard clinical protocols, including MOLLI-based native T_1 mapping, LGE imaging and CINE scans. LGE imaging was performed 10-15 minutes after injection of 0.15 mmol/kg of Gadobutrol (Gadovist, Bayer Schering). Extracellular volume (ECV) maps were estimated from native and postcontrast T_1 values. Synthetic hematocrit values were computed for each patient as $\mathrm{Hct} = 0.88 - (T_{1,\mathrm{blood}}/3240)$.[57] The proposed $T_{1\rho,\mathrm{adiab}}$ mapping sequence and conventional $T_{1\rho}$ mapping of a single mid-ventricular SAX slice were included in the scan protocol prior to contrast administration. Imaging parameters were chosen to closely match those used in the healthy subjects. PCA-based group-wise registration was used to mitigate residual cardiac and respiratory motion for baseline $T_{1\rho,\mathrm{adiab}}$ and $T_{1\rho}$ images.[58] T_1 and $T_{1\rho(,\mathrm{adiab})}$ baseline images were spatially co-registered to the corresponding LGE images applying a PCA-based group-wise method to the baseline images.[58] Finally, the resulting deformation matrices were transferred to the previously reconstructed maps. Manually drawn ROIs were defined on LGE images and then superimposed on the co-registered quantitative maps to extract scar and remote T_1, ECV, $T_{1\rho}$, and $T_{1\rho,\mathrm{adiab}}$ times.

3 | RESULTS

3.1 | Bloch simulations

The simulated preparation efficiency achieved with the 2HS-aSL, 4HS-aSL, and 8HS-aSL preparations is shown in Figure 3A. For all three modules, the highest preparation efficiency was obtained for low to intermediate frequency sweep amplitudes and showed an inversely proportional relationship with the parameter β. However, very low values of β required a reduction of the pulse peak power to satisfy SAR limitations. In all three cases, the optimal region is well-defined and separated from the non-adiabatic region at high sweep velocities (top-right corner). Overall, 2HS-aSL shows higher overall preparation efficiency than 4HS-aSL and 8HS-aSL. The 2HS-aSL module also presents a larger optimal region, indicating higher stability to the choice of parameters. Optimal values of $\{\beta, f_{\max}\}$ were chosen as $\{5.5, 350\ \mathrm{Hz}\}$ for 2HS-aSL, $\{3.7, 300\ \mathrm{Hz}\}$ for 4HS-aSL and $\{2.1, 550\ \mathrm{Hz}\}$ for 8HS-aSL, resulting in an average efficiency M_z/M_0 of 0.98 and 0.92 and 0.88, respectively. Hence, the 2HS-aSL configuration, consisting of 2 HS pulses of 30 ms each, was selected for further investigation.

Simulation results for 2HS-aSL preparation with three different design regions are shown in Figure 3B. For B_0-aSL and B_1-aSL, similar patterns to the previously analyzed Bal-aSL case (Figure 3A) can be observed, with an inversely proportional relationship with the parameter β. The optimal region becomes narrower when using a more B_1^+ compensated preparation, with overall decreasing optimal values β and $f_{\max}$. Optimal values of $\{\beta, f_{\max}\}$ were identified as $\{6.9, 450\ \mathrm{Hz}\}$ for B_0-aSL and $\{4.4, 200\ \mathrm{Hz}\}$ for B_1-aSL, yielding an average efficiency M_z/M_0 of 0.99 and 0.94, respectively. A summary of the parameters used for the optimized aSL preparations can be found in Table 1.

Figure 3C illustrates how the preparation efficiency $M_z(\tau_{\mathrm{SL}})/M(0)$ varies over a range of off-resonant frequencies and B_1^+ inhomogeneities for the optimized B_0-aSL, Bal-aSL and B_1-aSL modules according to Bloch simulations. The corresponding design region used for the parameter optimization of each preparation is marked by the dashed rectangle. For all three aSL modules, the regions characterized by low preparation efficiency (in blue) are outside the design region.

3.2 | Phantom and in vivo calf experiments

The experimental preparation efficiency measured in the phantom experiments with varying $\Delta\omega_1^{\mathrm{off}}$ and ζ_1

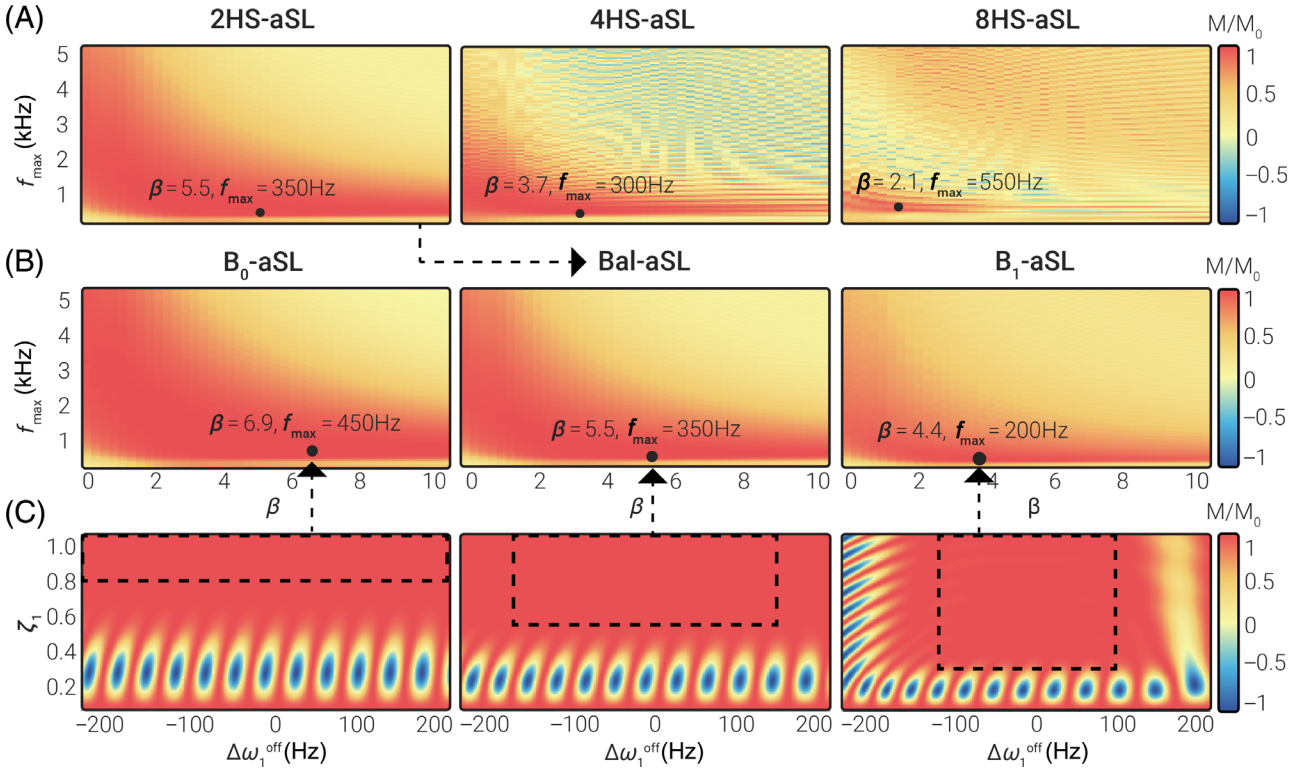

FIGURE 3 (A) Simulated preparation efficiency for 2HS-aSL, 4HS-aSL and 8HS-aSL preparations, obtained by concatenating 2 (τ_{HS} = 30 ms), 4 (τ_{HS} = 15 ms), or 8 (τ_{HS} = 7.5 ms) HS pulses, respectively. M_z/M_0 was averaged over a design window covering $\Delta\omega_1^{off} \in \{-150, -149, ... + 150\}$ Hz and $\zeta_1 \in \{0.50, 0.49, ...1.00\}$. Combinations of β and f_{max} yielding the highest efficiency are indicated for each module by a black dot. (B) Simulated preparation efficiency for 2HS-aSL, using three different design regions: B_0-aSL, Bal-aSL and B_1-aSL. Black dots mark the combination of β and f_{max} yielding the highest preparation efficiency. The highest efficiency was obtained for low f_{max} amplitudes and intermediate β. (C) Simulated preparation efficiency obtained for the optimal β and f_{max} combination identified in (B) for various $\Delta\omega_1^{off}$ and ζ_1. Dashed black boxes represent the design region considered for each pulse in (B).

TABLE 1 Adiabatic spin-lock preparations design parameters.

	Pulse shape				Design region		Performance	
Module name	β	f_{max} (Hz)	τ_{HS} (ms)	$B_1^{max}(\mu T)$	ω_1^{off} (Hz)	ζ_1	**SAR (W/kg)**	**Efficiency***
8HS-aSL	2.1	550	7.5	13.5	−150, … +150	0.5, … 1.0	<1.2	0.88
4HS-aSL	3.7	300	15	13.5	−150, … +150	0.5, … 1.0	<1.1	0.92
B_0-aSL (2HS-aSL)	6.9	450	30	13.5	−200, … +200	0.75, … 1.0	<1.0	0.99
Bal-aSL (2HS-aSL)	5.5	350	30	13.5	−150, … +150	0.5, … 1.0	<1.0	0.98
B_1-aSL (2HS-aSL)	4.4	200	30	13.5	−100, … +100	0.25, … 1.0	<1.1	0.94

* $M_z(\tau_{SL})/M(0)$ averaged over design region.

conditions is depicted in Figure 4A. Good agreement between the simulated and experimental results can be observed. Broad areas of lower preparation efficiency are present for intermediate to low ζ_1 values with B_0-aSL, low to very-low ζ_1 values with Bal-aSL, and very low ζ_1 as well as high absolute $\Delta\omega_1^{off}$ values with B_1-aSL.

The results in terms of preparation efficiency obtained in vivo in the calf muscle of a healthy subject are shown in Figure 4B. These results are in good agreement with both simulations and phantom data. In vivo preparation efficiency is compromised for $\zeta_1 < 0.6$ with the B_0-aSL module, while no substantial degradation was observed over the entire off-resonance range studied. On the opposite side, B_1-aSL yields robust preparation efficiency for ζ_1 values down to 0.2, but lower efficiency for $|\Delta\omega_1^{off}| > 150$ Hz. The overall efficiency score measured in the phantom

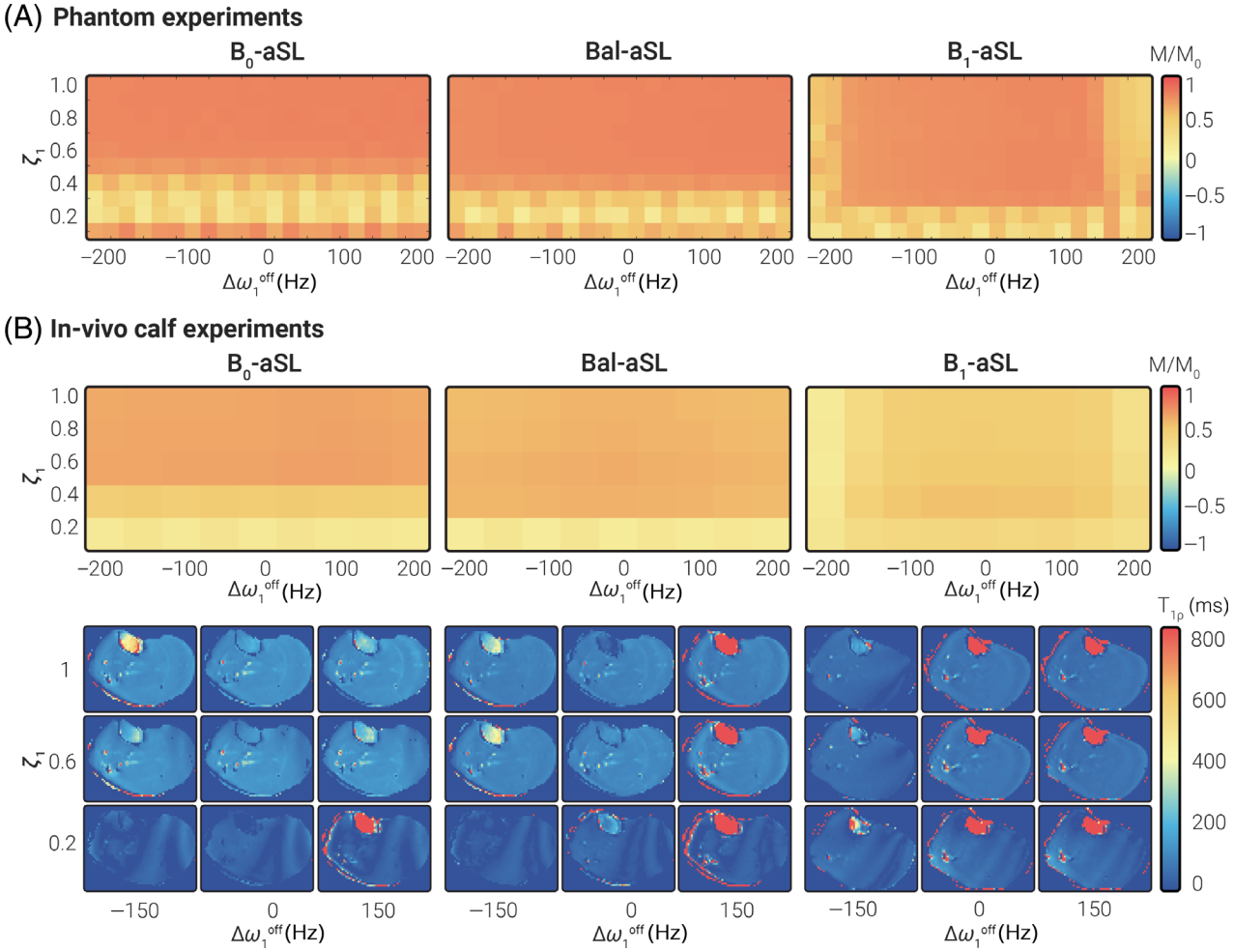

FIGURE 4 (A) Experimental preparation efficiency measured in phantoms for a range of $\Delta\omega_1^{off}$ and ζ_1 with three adiabatic spin-lock (aSL) preparations. Experimental results were in agreement with simulations in Figure 3C, minus a scaling factor given by relaxation, which was ignored in simulations. (B) Adiabatic preparations efficiency was measured in vivo on a healthy subject's calf muscle for the same range of $\Delta\omega_1^{off}$ and ζ_1. Overall, the results were in good agreement with the phantom experiments (A) and the numerical simulations (Figure 3C). Representative calf $T_{1\rho,adiab}$ maps for different values of $\Delta\omega_1^{off}$ and ζ_1 illustrate the variation in image artifacts.

and calf experiments is lower than in simulations, as no relaxation contributions have been simulated.

Complete $T_{1\rho}$ and $T_{1\rho,adiab}$ mapping results for the T1MES phantom can be found in Figure S2. Improved repeatability was observed ($p < 0.05$) in $T_{1\rho,adiab}$ maps ($\overline{wCV_i} = 0.29 \pm 0.15\%$ for B_0-aSL, $p < 0.01$; $\overline{wCV_i} = 0.23 \pm 0.13\%$ for Bal-aSL, $p < 0.01$; $\overline{wCV_i} = 0.21 \pm 0.11\%$ for B_1-aSL, $p < 0.001$) with respect to conventional $T_{1\rho}$ maps ($\overline{wCV_i} = 1.30 \pm 1.34\%$ for RefSL).

In Figure 5, examples of phantom and calf $T_{1\rho,adiab}$ maps acquired with different β values are displayed. $T_{1\rho,adiab}$ values increase with an approximately linear trend for higher β in both cases ($R^2 = 0.99$, slope = 9.56, intercept = 32.15 for phantoms, $R^2 = 0.91$, slope = 12.46, intercept = 26.53 for the calf). A higher deviation from linearity was observed in the calf values for $\beta \in \{3, 4, 5\}$.

3.3 | Healthy subjects experiments

Figure 6A shows mid-ventricular SAX and four-chamber $T_{1\rho,adiab}$ maps for one representative subject, displaying overall strong myocardium-to-blood contrast. No major off-resonance or B_1^+ artifacts are visually apparent on the $T_{1\rho,adiab}$ maps. In agreement with phantom and calf results, myocardial $T_{1\rho,adiab}$ values obtained with the B_0-aSL preparation ($\beta = 6.9$) are higher than those obtained with the Bal-aSL preparation ($\beta = 5.5$), which in turn are higher than those obtained with B_1-aSL preparations ($\beta = 4.4$). Myocardial $T_{1\rho,adiab}$ values averaged over slices, segments, and subjects were 194.22 ± 24.54 ms, 155.59 ± 18.09 ms, and 87.48 ± 11.55 ms for B_0-aSL, Bal-aSL, and B_1-aSL, respectively. The bull's-eye plots in Figure 6B show that the inter-subject average $T_{1\rho,adiab}$ values for all three aSL

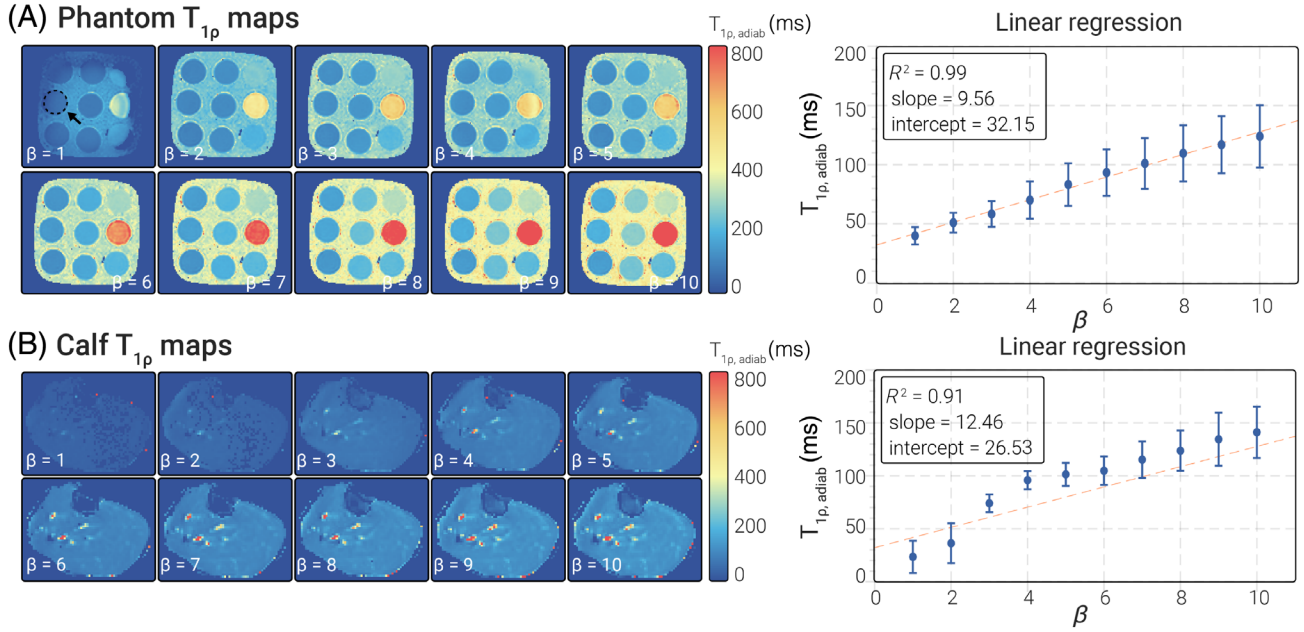

FIGURE 5 (A) Phantom and (B) calf $T_{1\rho,adiab}$ maps were obtained for various β and constant $f_{max} = 350$ Hz. Linear regression analysis results showed that both phantoms and calf present a linear relationship between the pulse β and the measured $T_{1\rho,adiab}$ values.

preparations are homogeneous across all segments. Bal-aSL and B_1-aSL bullseye plots depict lower $T_{1\rho,adiab}$ values in the apical slice (apical vs. basal slice: −2.64%, $p < 0.001$ for Bal-aSL, −6.62%, $p < 0.001$ for B_1-aSL) but not for B_0-aSL (−0.97%, $p = 0.12$).

Figure 6C depicts good reproducibility across the 16 AHA segments for all aSL preparations. Trends of improved precision and reproducibility were observed for B_0-aSL compared with B_1-aSL, but the differences were not significant ($p > 0.08$). However, B_0-aSL yielded significantly lower inter-subject variability than B_1-aSL ($p < 0.05$).

B_0-aSL $T_{1\rho,adiab}$ and RefSL $T_{1\rho}$ maps obtained in two repetitions under different shimming conditions for a representative subject are shown in Figure 7. RefSL preparations yield lower $T_{1\rho}$ values than B_0-aSL (average $T_{1\rho}$ over subjects, slices and segments = 38.21 ± 14.37 ms for RefSL, compared with 183.28 ± 25.53 ms for B_0-aSL, Figure 8A). RefSL-based $T_{1\rho}$ maps display pronounced artifacts over large portions of the myocardium and poor reproducibility across the shimming conditions. B_0-aSL preparations, on the other hand, present comparable image quality for both cases, free of visually apparent artifacts. The adiabatic B_0-aSL preparation resulted in significantly better precision compared with RefSL (B_0-aSL: $wCV_{i,r}$ = 14.51 ± 3.71%, RefSL: $wCV_{i,r}$ = 37.61 ± 19.42%; $p < 0.01$, Figure 8C).

At least 10 times higher reproducibility was obtained with the B_0-aSL preparation compared with the RefSL module (average $\overline{wCV}_i$ = 4.64 ± 2.18% for B_0-aSL against average $\overline{wCV}_i$ = 47.39 ± 12.06% for RefSL, $p < 0.0001$), as shown in Figure 8C.

Finally, inter-subject variability was lower for the B_0-aSL preparation ($\overline{CV}$ = 8.76 ± 3.65% for B_0-aSL), compared with the conventional SL ($\overline{CV}$ = 51.90 ± 15.27% for RefSL, $p < 0.0001$), as shown in Figure 8C.

A complete overview of the in vivo myocardial $T_{1\rho,adiab}$ and $T_{1\rho}$ values, as well as precision, reproducibility, and inter-subject variability for each healthy subject across the two cohorts, can be found in Tables S1–S4.

3.4 | Patients experiments

Four of the six patients presented as LGE-positive in the CMR. For two of those four patients, the mid-SAX slice intersected with the area of focal scar identified on the LGE images. Figure 9 shows the clinical sequences as well as aSL-based $T_{1\rho,adiab}$ maps and RefSL-based $T_{1\rho}$ maps for the two subjects with LGE-identified scars in the mid-ventricular SAX slice. $T_{1\rho,adiab}$ maps show visually discernable alteration in the myocardium, that spatially coincides with the areas of hyper-enhancement in the LGE images. Any potential alteration in the RefSL-based $T_{1\rho}$ maps is obfuscated by the presence of substantial artifacts. B_1-aSL yielded the best maps quality among adiabatic preparations, with no visible B_0 or B_1^+-related artifacts. B_0-aSL and Bal-aSL maps were characterized by overall lower quality and presented visible artifacts across the myocardium, as shown in Figure S3.

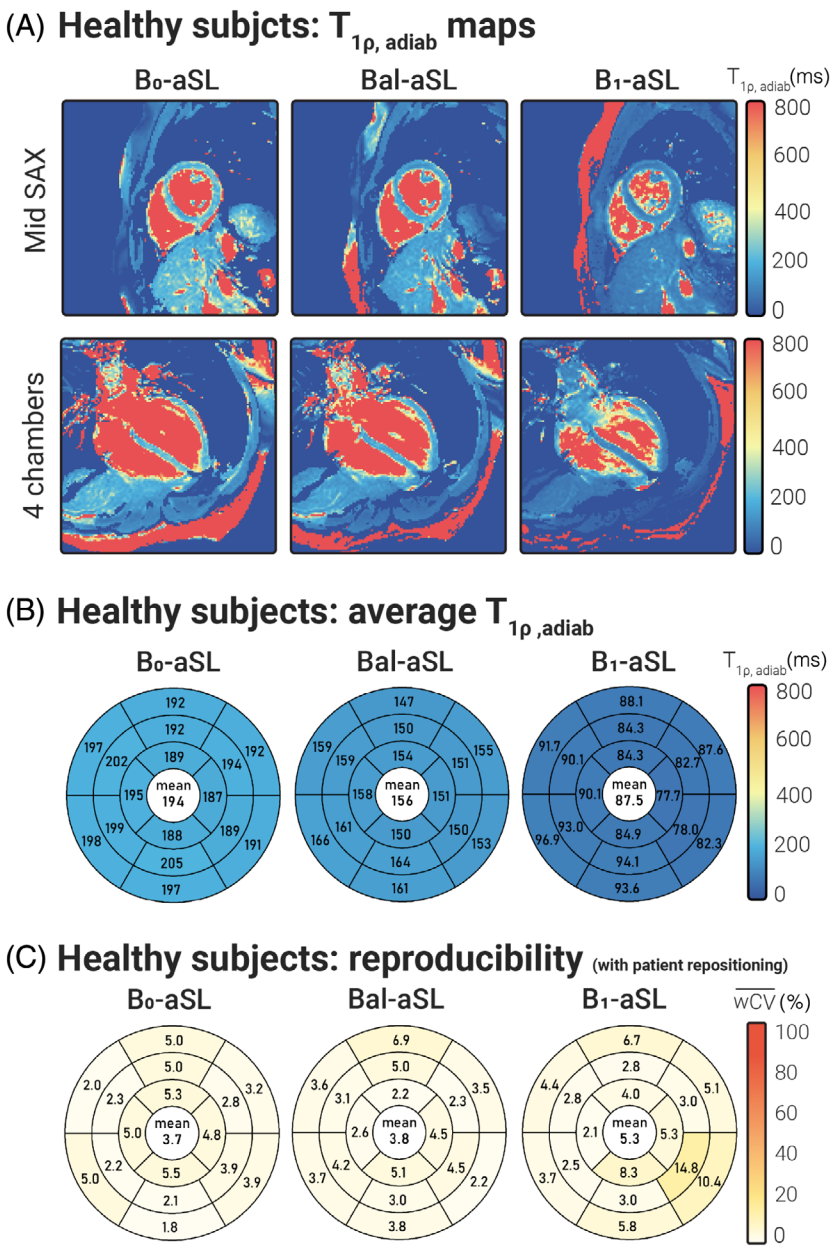

FIGURE 6 (A) Mid SAX and four-chamber $T_{1\rho,adiab}$ maps obtained with B_0-aSL, Bal-aSL, and B_1-aSL preparations in a representative healthy subject of the first cohort. $T_{1\rho,adiab}$ maps achieved good visual map quality, with a homogeneous myocardium and clear delineation against the blood pool across all acquired slices. (B) Bull's-eye plots showing the $T_{1\rho,adiab}$ values, averaged over all subjects and repetitions, for 16 AHA myocardial segments. $T_{1\rho,adiab}$ values are homogeneous across the 16 segments for all preparations. Average $T_{1\rho,adiab}$ increases with increasing beta β. (C) Bullseye plots report the average reproducibility ($\overline{wCV}$) coefficients, measured over two acquisitions interleaved by subject repositioning, for adiabatic spin-lock (aSL)-prepared maps in 16 AHA myocardial segments. Global average values are reported at the center of each bullseye plot. A mild improvement in reproducibility is observed for B_0-aSL and Bal-aSL preparations, compared to B_1-aSL, but the difference was not statistically significant ($p > 0.05$).

Patient 1 shows near transmural enhancement in the LGE images. $T_{1\rho,adiab}$ in this subject shows a +47.48% elevation in the LGE-positive area compared with the remote myocardium for B_1-aSL, while RefSL-based $T_{1\rho}$ maps show a −33.26% difference. In comparison, native T_1 and ECV values for the same patient showed, respectively, +17.12% and +80.53% in the LGE-positive area. In patient 2, who showed signs of lipomatous metaplasia in bSSFP CINE images (Figure 9), decreased relaxation times were measured for the LGE positive area, compared with remote healthy myocardium (−6.04% for B_1-aSL $T_{1\rho,adiab}$, −67.19% for RefSL $T_{1\rho}$, −3.11% for native T_1, −41.19% for ECV), as expected in the presence of fatty infiltration. Major artifacts, however, impair the T_1 and ECV maps quality. For both patients, normal $T_{1\rho,adiab}$ and $T_{1\rho}$ values were measured in the remote myocardium (202.18 ± 17.79, 169.42 ± 13.06, 97.98 ± 11.35, and 42.91 ± 17.81 ms for B_0-aSL, Bal-aSL, B_1-aSL, and RefSL, respectively). Normal $T_{1\rho,adiab}$ and $T_{1\rho}$ values were also measured in LGE-negative patients (191.32 ± 13.53, 148.46 ± 12.95, 92.35 ± 7.29, and 33.59 ± 14.36 ms for B_0-aSL, Bal-aSL, B_1-aSL, and RefSL, respectively).

4 | DISCUSSION

In this study, we proposed a new cardiac $T_{1\rho,adiab}$ mapping technique based on fully aSL preparation for myocardial tissue characterization at 3T. Numerical optimization yielded aSL preparations with tuneable resilience

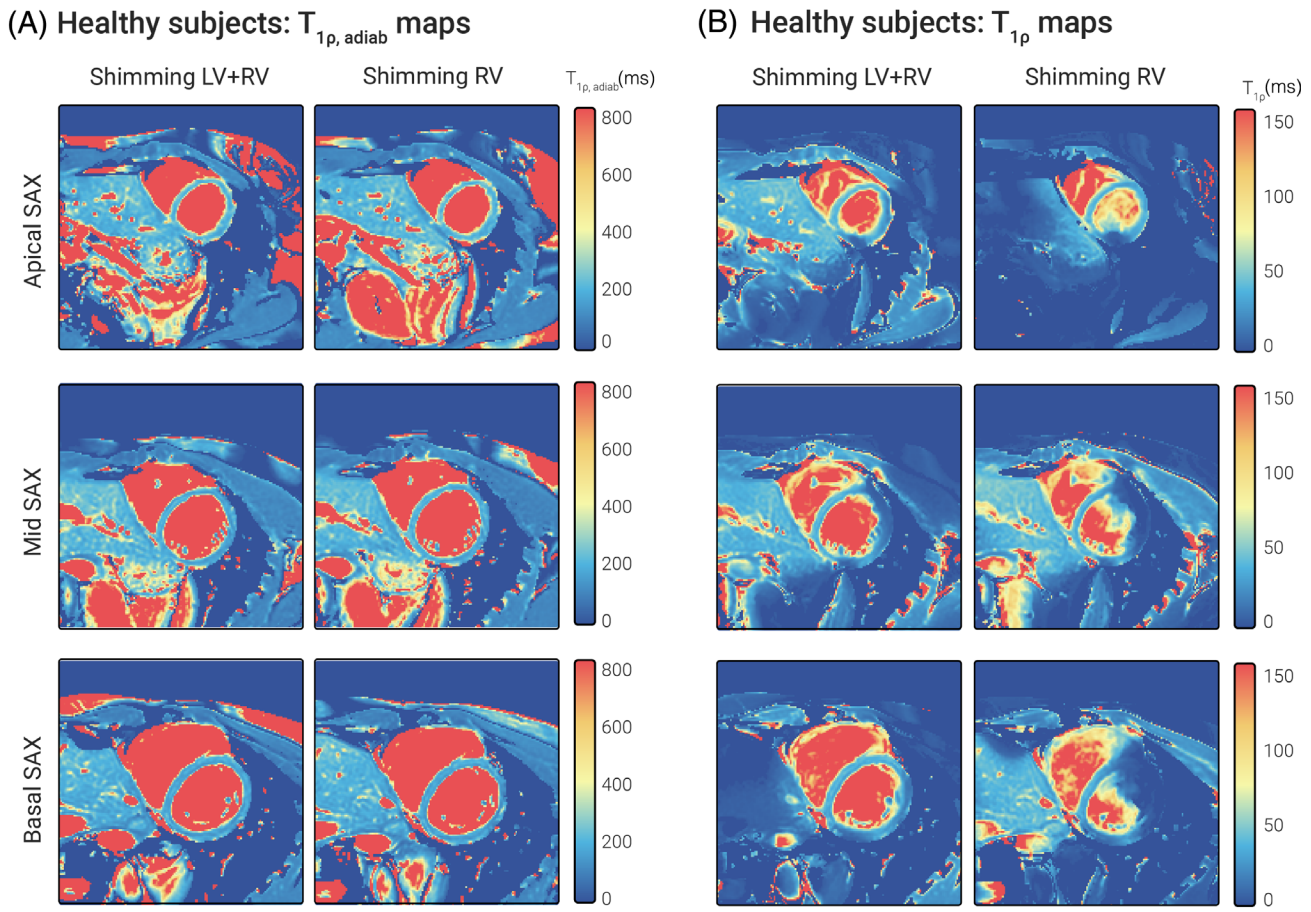

FIGURE 7 Apical, mid, and basal short-axis (A) B_0-aSL-prepared $T_{1\rho,adiab}$ maps and (B) RefSL-prepared $T_{1\rho}$ maps in a representative healthy subject. Two repetitions of each slice and preparation were acquired with different shim volumes: one covering the entire heart, the other covering only the right ventricle. $T_{1\rho,adiab}$ maps retain comparable map quality across repetitions with a nearly identical visual appearance of the maps. RefSL maps depict significant artifacts degrading the map quality in the myocardium, particularly in the second repetition.

against B_0 and B_1^+ inhomogeneities. Phantom and in vivo measurements demonstrated that $T_{1\rho,adiab}$ mapping achieved more robust results than conventional $T_{1\rho}$ mapping approaches. $T_{1\rho,adiab}$ maps showed fewer artifacts, higher precision and reproducibility, and lower inter-subject variability. Initial data showed feasibility in patients and visual alignment of areas with altered $T_{1\rho,adiab}$ and hyper-enhancement in LGE images.

Conventional $T_{1\rho}$ values obtained with the RefSL preparation in this study were comparable to those reported in previous studies at 3T.[31-33] However, our results show slightly lower precision for the RefSL maps than in previous studies. This difference in variability may be because previous studies only evaluated a small ROI in the anteroseptal segment of the myocardium, while in this work, an automatic segmentation of the entire myocardium was used. Significant inhomogeneities are visible in conventional RefSL maps, both in our results and in other studies.[31-33] Han et al. found that at 1.5T B_0 variations over 10% of the SL field amplitude (typically $B_1/\gamma = 500$ Hz) cause $T_{1\rho}$ quantification errors and visible image artifacts.[35] At 3T, this limit is easily exceeded.[39] Furthermore, B_1^+ inhomogeneities have a much higher impact at high fields in cardiac imaging,[48] thus necessitating more robust $T_{1\rho}$ mapping techniques.

Both adiabatic and conventional $T_{1\rho}$ maps showed lower $T_{1\rho,adiab}$ or $T_{1\rho}$ values in the apical slice, compared to the mid and basal slices. This effect is less evident for the B_0-aSL preparations ($T_{1\rho,adiab}$ values comparison apical vs. mid and basal slices: $p = 0.77$ for B_0-aSL, $p < 0.01$ for B_1-aSL and Bal-aSL, Figure 6). Hence, the lower $T_{1\rho,adiab}$ and $T_{1\rho}$ values in the apical slice may be explained with the higher contribution of B_0 inhomogeneities at the apex.

Using fully aSL preparations has four major advantages. First, they yield more robust $T_{1\rho,adiab}$ quantification in the presence of field inhomogeneities. Our results have shown that the $T_{1\rho,adiab}$ maps have a lower level of noise and do not present significant B_0- or B_1^+-related artifacts, overcoming the limitations observed in the previous studies.[31-33] $T_{1\rho,adiab}$ preparations also yielded higher

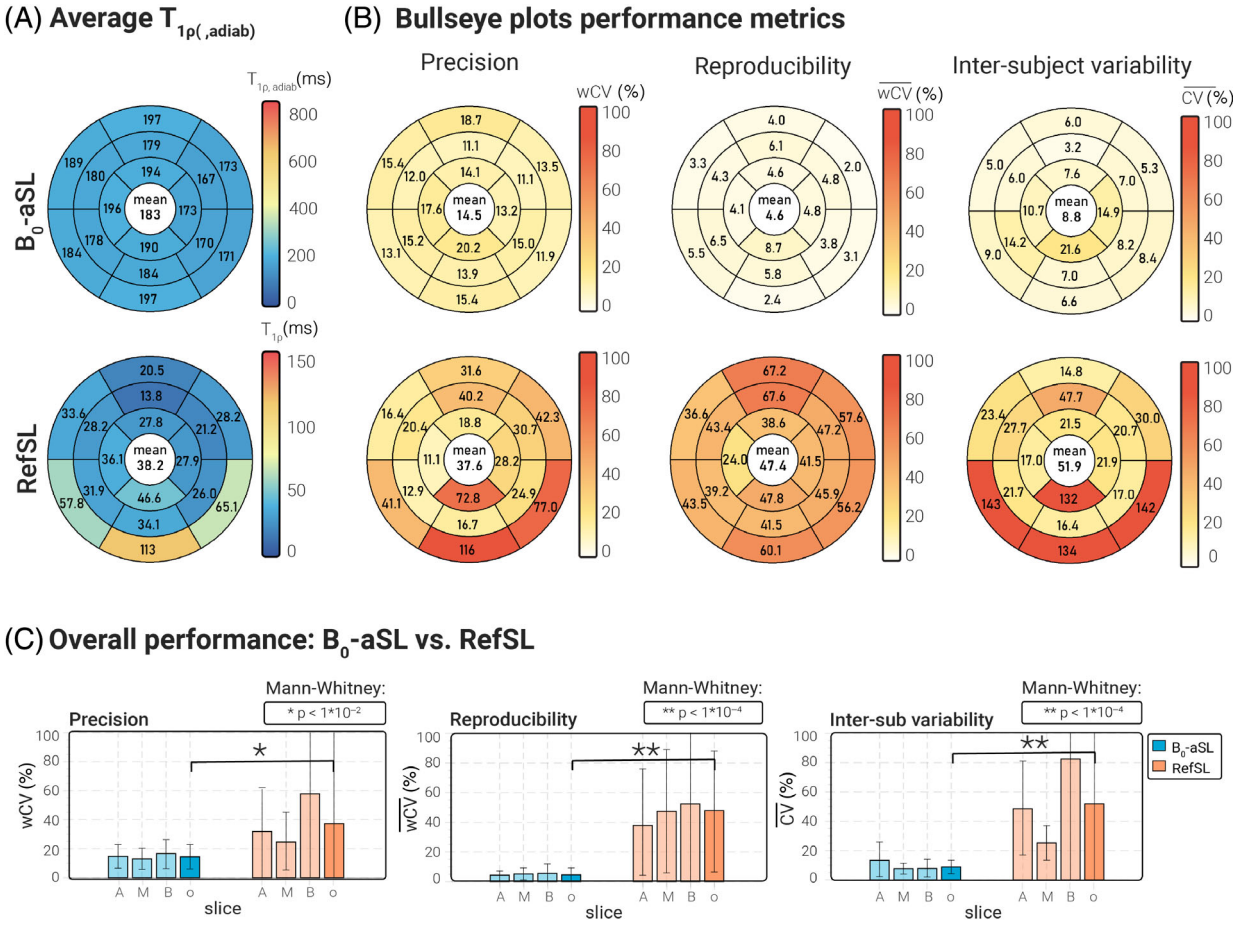

FIGURE 8 (A) Bull's-eye plots showing the $T_{1\rho,adiab}$ and $T_{1\rho}$ values, averaged over all cohort two subjects and repetitions, for 16 AHA myocardial segments. $T_{1\rho,adiab}$ values are consistently higher, but more homogeneous across the 16 segments for all preparations, compared with RefSL-based $T_{1\rho}$ values. (B) Bullseye plots report the average precision (wCV), reproducibility ($\overline{wCV}$), and inter-subject variability ($\overline{CV}$) coefficients for B_0-aSL-based $T_{1\rho,adiab}$ maps and RefSL $T_{1\rho}$ maps in 16 AHA myocardial segments. Global average values are reported at the center of each bull's-eye plot. Improved precision, reproducibility, and inter-subject variability are obtained with aSL preparations, compared to RefSL. (C) Bar plots comparing precision, reproducibility, and inter-subject variability for each preparation per slice and averaged across all slices (A = apical, M = mid-ventricular, B = basal, o = overall). Pair-wise statistical significance is marked by ∗ or ∗∗ and the corresponding p-values are shown on top of each plot. Significantly higher $wCV_{r,i}$, $\overline{wCV}$, and $\overline{CV}$ values are measured for conventional RefSL-based $T_{1\rho}$ mapping compared with $T_{1\rho,adiab}$.

precision, reproducibility, and lower inter-subject variability. Resilience to artifacts is of particular importance for applications at high field strengths, like 3T, which have the potential advantage of increased signal-to-noise ratio and CNR. Second, the use of amplitude-modulated HS pulses lowers the SAR demands compared to conventional continuous-wave preparations for the same duration. Wang et al. reported a SL pulse amplitude B_1/γ of 298 Hz,[33] limited by SAR constraints and comparable with our findings. Low SL pulse amplitudes result in lower measured $T_{1\rho}$ values and further compromise the CNR and robustness to system imperfections. The aSL pulses used in this study, on the other hand, allowed us to use maximum peak power and longer preparation times, while still satisfying SAR limitations. Third, $T_{1\rho,adiab}$ preparations eliminate the need for the initial 90° tip of the magnetization, which introduces further imperfections in the presence of B_1^+ inhomogeneities.[42,51] Finally, conventional SL preparations are orientation dependent.[59] The high anisotropy of myocardial fibers yields orientation-dependent $T_{1\rho}$ times with conventional preparations.[60] Adiabatic $T_{1\rho}$ preparations, on the other hand, have been shown to be orientation independent.[59] This may further contribute to more homogeneous and reproducible $T_{1\rho,adiab}$ maps across the myocardium.

Besides the advantages in terms of robustness given by aSL preparations, the mechanism behind $T_{1\rho,adiab}$ relaxation is intrinsically different from conventional $T_{1\rho}$. Each $T_{1\rho,adiab}$ preparation probes a wider spectrum of SL frequencies through the adiabatic sweep, compared to mono-frequency conventional SL. Effective field strength and orientation vary during aSL preparations, as well as

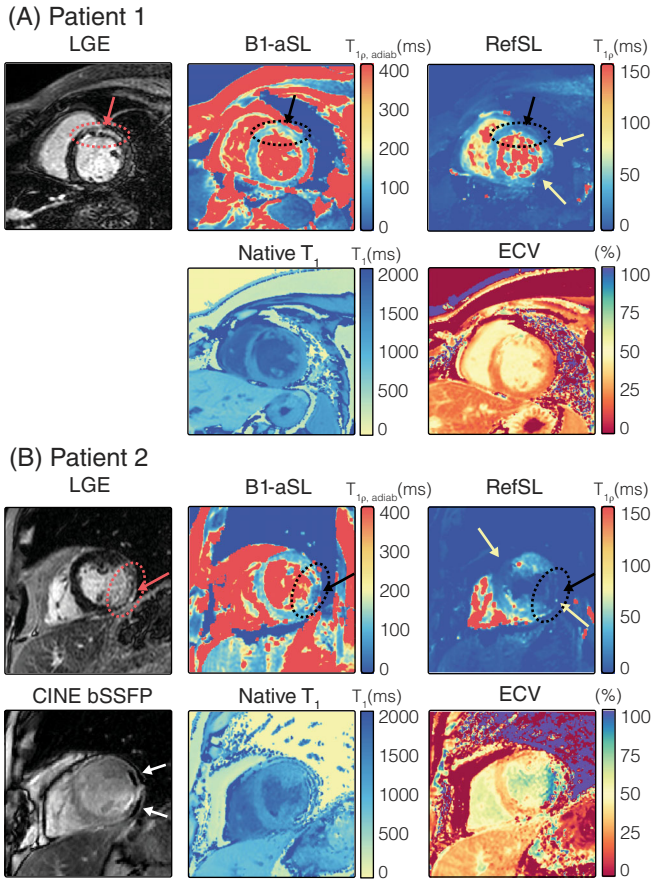

FIGURE 9 (A) 53-year-old female patient suffering from ischemic cardiomyopathy. LGE images demonstrate myocardial infarction in the mid anteroseptal and anterior wall. A circular ghosting artifact is visible on the LGE image and partially overlaps with myocardial scar (red arrow). The B_1-aSL-based $T_{1\rho,adiab}$ map shows elevation co-localized with LGE positive regions ($T_{1\rho,adiab}$ = 146.24 ± 25.34 scar -black arrow-, 99.40 ± 11.58 remote). Native T_1 and ECV values are also focally elevated in the anterior and anteroseptal segments. Due to changes in the imaging slice position, however, the visible abnormalities in native T_1 maps are not precisely co-localized with the LGE positive area. Due to mapping inhomogeneity in the anterior and lateral regions (yellow arrows), no focal alteration is unambiguously identified in the conventional $T_{1\rho}$ maps. (B) 59-year-old male patient with a history of ischemic cardiomyopathy. LGE images demonstrate transmural myocardial enhancement in the mid-anterolateral segments (red arrow). Chemical shift artifacts in the bSSFP CINE images indicate lipomatous metaplasia. $T_{1\rho,adiab}$ values decrease in the scar region ($T_{1\rho,adiab}$ = 67.06 ± 14.69 scar -black arrow-, 96.57 ± 15.03 remote). Native T_1 and ECV values are also lower in correspondence of the scar region with respect to remote myocardium, although major artifacts impair the quality of the maps. In this patient, significant artifacts obfuscate any potential focal alteration in the RefSL-based $T_{1\rho}$ maps (yellow arrows).

the angle between the effective field and the magnetization. These variations lead to relaxation rate changes throughout the preparation module, rather than sampling a uniform $T_{1\rho}$.[43,44] On the other hand, the variable transverse relaxation $T_{2\rho}$ contribution in the rotating frame of reference results in different $T_{1\rho}/T_{2\rho}$ ratios for any given time point. Furthermore, we observed higher $T_{1\rho,adiab}$ times for preparations with higher β and, thus, a faster frequency sweep velocity. This indicates that the spectrum of relaxations rates probed during aSL varies depending on the pulse profiles. These factors may lead to a different sensitivity profile in pathological remodeling and its clinical value remains to be evaluated. An in-depth theoretical analysis of the mechanisms behind $T_{1\rho,adiab}$ relaxation would be beneficial for the comprehension of its relationship with the underlying physiology.

In patients, the poor resilience of RefSL preparations to system imperfections significantly compromised the map quality. Artifacts in the area around the coronary sinus, as well as the lateral wall, appeared in all cases, preventing the unambiguous identification of focal alteration. Compared to healthy subjects, image artifacts were substantially more pronounced in the patient cohort. This likely stemmed from lower B_1^+ shim quality in the clinical setting. aSL-based preparations, in particular when tuned for B_1^+-resilience, yielded good map quality, comparable to the healthy subject cohort. This indicates fair resilience to system imperfections in clinical use.

Cardiac $T_{1\rho,adiab}$ maps showed visible focal alteration that spatially coincided with areas of hyper-enhancement in the LGE images. This is in line with previous studies indicating sensitivity to a range of diseases. Wang et al. found a +24% $T_{1\rho}$ elevation for hypertrophic cardiomyopathy patients with diffuse fibrosis.[33] At 1.5T, van Oorschot et al. measured +52% $T_{1\rho}$ elevation in infarcted myocardium of patients suffering from ischemic heart disease and +46% in a second ischemic cohort.[27] Furthermore, Bustin et al. have found a +40% elevation in infarcted myocardium of LGE-positive patients.[29] These trends are in agreement with the $T_{1\rho,adiab}$ enhancement measured in patient 1. On the other hand, $T_{1\rho,adiab}$ in the scar area of patient 2 was decreased. This is in good agreement with the CMR finding of lipomatous metaplasia,[61-63] and expected in these cases due to the short $T_{1\rho,adiab}$ component of the intramyocardial fat. Our preliminary results indicate that fully adiabatic $T_{1\rho}$ mapping can potentially yield more robust quantification than conventional continuous-wave SL in clinical use at high fields. However, clinical sensitivity of $T_{1\rho,adiab}$ mapping may differ from conventional continuous wave $T_{1\rho}$ mapping due to the mechanistic differences and among different adiabatic

preparations due to differences in the effective and fictitious fields. Consequently, larger dedicated cohorts of healthy controls and a targeted patient population are warranted to determine clinical sensitivity and potential cut-off values for the differentiation of healthy and infarcted myocardium.

Pulse design optimization was the key to achieving the desired resilience against B_0 and B_1^+ inhomogeneities. The HS pulse shape was chosen specifically for its enhanced resilience to B_0 inhomogeneities, superior to TANH/TAN pulses, as previously reported.[39] First, we observed that shorter aSL pulses (4HS-aSL and 8HS-aSL) performed worse than the longer one (2HS-aSL) despite allowing for complete Malcolm–Levitt compensation. Longer HS pulses are thus preferred for $T_{1\rho,adiab}$ preparations. Second, we found that the optimal HS pulse shape varies significantly under different B_0 and B_1^+ conditions. Bloch simulations were in very good agreement with the experimental data acquired in both the phantoms and the calf muscle. Our in vivo results show that B_0-aSL preparations achieve better precision and inter-subject variability than Bal-aSL and B_1-aSL in healthy subjects. However, B_1-aSL has proven most robust in the clinical setup where B_1-shim quality was reduced.

Increased $wCV_{r,i}$, $\overline{wCV_i}$, and $\overline{CV}$ values were observed in the basal and mid-inferolateral segment, as well as the apical lateral segment for B_1-aSL preparations (see Figure 8). These values were reflected in the B_1-aSL $T_{1\rho,adiab}$ maps, which, for some subjects, presented residual B_0 artifacts in the same segments (Figure 7). These effects were not observed for B_0-aSL and Bal-aSL maps. Thus, depending on the application and the technical characteristics of the scanner either of the optimized preparations may be most suitable for robust $T_{1\rho,adiab}$ quantification in the clinic. Adiabatic pulses that were previously used for other cardiac MRI applications were found to be closest to those used for B_1-aSL preparations ($\beta = 4.8$, $f_{max} = 215$ Hz[40]). These pulses may be particularly warranted on systems where B_1 quality is the main concern, such as systems with a single transmit channel or a lack of advanced shim modes. On other systems, B_0-aSL and Bal-aSL preparations may be preferred for the observed increase in precision and reproducibility.

In our study, patient scans showed pronounced cardiac and respiratory motion, despite cardiac triggering and breath-holding. Residual motion due to heart rate variability and poor breath-holding capacity in patients rendered retrospective image registration necessary to achieve satisfactory map quality in the final $T_{1\rho,adiab}$ and $T_{1\rho}$ maps. Recently, specific attention has been dedicated to the development of accelerated, free-breathing, whole-heart $T_{1\rho}$ mapping sequences to facilitate its clinical implementation.[28,64,65] Furthermore, several motion correction approaches have been proposed to improve the quality of reconstructed $T_{1\rho}$ maps and mitigate the contribution of motion.[26,29] These efforts are key to enabling the widespread use of quantitative parametric mapping sequences in clinical practice. Our aSL preparations are fully compatible with these sequence designs and reconstruction approaches and could, in the future, be integrated into accelerated and motion-corrected $T_{1\rho}$ mapping sequences. This may be particularly helpful to facilitate testing of the proposed $T_{1\rho,adiab}$ mapping in large, relevant patient cohorts in order to demonstrate its clinical value.

5 | CONCLUSIONS

In this work, $T_{1\rho,adiab}$ mapping was proposed as an alternative to conventional $T_{1\rho}$ mapping to enable its application in the human myocardium at 3T. Our results show that aSL preparations enable more robust mapping in the presence of B_0 and B_1^+ inhomogeneities while satisfying SAR limitations. Adiabatic preparation modules yielded quantification with high precision and reproducibility in healthy subjects. In patients, aSL-based $T_{1\rho,adiab}$ maps depicted focal alterations in agreement with the reference LGE scans. Thus, $T_{1\rho}$ mapping can be a promising candidate for reproducible myocardial tissue characterization and bears potential as a contrast-free imaging biomarker for scar and fibrosis.

ACKNOWLEDGMENTS

We would like to thank Paul de Bruin, Ece Ercan, and David Higgins for their help in facilitating the patient scans. We also thank Jouke Smink for his valuable input regarding the pulse sequence development.

ORCID

Chiara Coletti https://orcid.org/0000-0001-5994-2834
Anastasia Fotaki https://orcid.org/0000-0002-0353-5778
Joao Tourais https://orcid.org/0000-0002-1388-4023
Mehmet Akçakaya https://orcid.org/0000-0001-6400-7736
Qian Tao https://orcid.org/0000-0001-7480-0703
Claudia Prieto https://orcid.org/0000-0003-4602-2523
Sebastian Weingärtner https://orcid.org/0000-0002-0739-6306

REFERENCES

1. Kim RJ, Ling CE, Lima João AC, Judd RM. Myocardial Gd-DTPA kinetics determine MRI contrast enhancement and reflect the extent and severity of myocardial injury after acute reperfused infarction. *Circulation*. 1996;94:3318-3326.

2. Kim RJ, Edwin W, Allen R, et al. The use of contrast-enhanced magnetic resonance imaging to identify reversible myocardial dysfunction. *N Eng J Med*. 2000;343:1445-1453.
3. Kim HW, Afshin F-F, Kim RJ. Cardiovascular magnetic resonance in patients with myocardial infarction. Current and emerging applications. *J Am Coll Cardiol*. 2009;55:1-16.
4. Prabhakar R, Desai MY, Deborah K, Flamm SD. MR imaging of myocardial infarction. *Radiographics*. 2013;33:1383-1412.
5. Hassan A-A, Anja Z, Jeanette S-M, et al. Delayed enhancement and T2-weighted cardiovascular magnetic resonance imaging differentiate acute from chronic myocardial infarction. *Circulation*. 2004;109:2411-2416.
6. Elena L, Svetlana K, Vincent L-V, Nicolas J, Gilbert D. Renal safety of gadolinium-based contrast media in patients with chronic renal insufficiency. *Radiology*. 2009;250:618-628.
7. Tomonori K, Kazunari I, Hiroki K, Kazuhiro K, Daisuke T. High signal intensity in the dentate nucleus and globus pallidus on unenhanced T1-weighted MR images: relationship with increasing cumulative dose of a gadoliniumbased contrast material. *Radiology*. 2014;270:834-841.
8. Ismail TF, Wendy S, Chiara C, et al. Cardiac MR: from theory to practice. *Front Cardiovasc Med*. 2022;0:137.
9. Erica DA, Piechnik Stefan K, Ferreira Vanessa M, et al. Cardiovascular magnetic resonance by non contrast T1-mapping allows assessment of severity of injury in acute myocardial infarction. *J Cardiovasc Magn Reson*. 2012;14:1-13.
10. David C, Caroline H, Sam R, et al. Prognostic significance of infarct core pathology revealed by quantitative non-contrast in comparison with contrast cardiac magnetic resonance imaging in reperfused ST-elevation myocardial infarction survivors. *Eur Heart J*. 2016;37:1044-1059.
11. Shiro N, Javid A, Steven B, et al. Native T1 value in the remote myocardium is independently associated with left ventricular dysfunction in patients with prior myocardial infarction. *J Magn Reson Imaging*. 2017;46:1073-1081.
12. Martin U, Bagi PS, Oki AJ, et al. Myocardial edema as detected by pre-contrast T1 and T2 CMR delineates area at risk associated with acute myocardial infarction. *JACC Cardiovasc Imaging*. 2012;5:596-603.
13. Stoffers RH, Marie M, Mohammed S, et al. Assessment of myocardial injury after reperfused infarction by T1ρ cardiovascular magnetic resonance. *J Cardiovasc Magn Reson*. 2017;19:1-10.
14. Emily A, Kelvin C, James C. Cardiac T1 mapping: techniques and applications. *J Magn Reson Imaging*. 2020;51:1336-1356.
15. Martino AF, Damadian R. Improved discrimination of normal and malignant tissue using 1H NMR relaxation time measurements at 2.18 MHz. *Physiol Chem Phys Med NMR*. 1984;16:49-55.
16. Sepponen RE, Pohjonen JA, Sipponen JT, Tanttu JI. A method for T1 rho imaging. *J Comput Assist Tomogr*. 1985;9:1007-1011.
17. Raja M, Flamm SD, Wilson JM, Pettigrew RI, Thomas DW. Acute myocardial infarction: tissue characterization with T1 ρ-weighted MR imaging - initial experience. *Radiology*. 2004;232:606-610.
18. Steffen H, Raja M, Brenda L, Mercedes P, Alicia N, Flamm SD. Tissue characterization of myocardial infarction using T1ρ: influence of contrast dose and time of imaging after contrast administration. *J Magn Reson Imaging*. 2006;24:1040-1046.
19. Witschey Walter RT, Pilla JJ, Giovanni F, et al. Rotating frame spin lattice relaxation in a swine model of chronic, left ventricular myocardial infarction. *Magn Reson Med*. 2010;64:1453-1460.
20. Rt WW, Zsido GA, Kevin K, et al. In vivo chronic myocardial infarction characterization by spin locked cardiovascular magnetic resonance. *J Cardiovasc Magn Reson*. 2012;14:1-9.
21. Musthafa Haja Sherief N, Galina D, Line L, et al. Longitudinal rotating frame relaxation time measurements in infarcted mouse myocardium in vivo. *Magn Reson Med*. 2013;69:1389-1395.
22. Maximilian G, Daniel G, Patrick W, et al. Fast myocardial T 1ρ mapping in mice using k-space weighted image contrast and a Bloch simulation-optimized radial sampling pattern. *Magn Resonan Mater Phys Biol Med*. 2022;35:325-340.
23. Maximilian G, Daniel G, Petra A, et al. Quantification correction for free-breathing myocardial T1ρ mapping in mice using a recursively derived description of a T1ρ* relaxation pathway. *J Cardiovasc Magn Reson*. 2022;24:1-16.
24. Zhang Y, Wen Z, Wei C, et al. MR extracellular volume mapping and non-contrast T1ρ mapping allow early detection of myocardial fibrosis in diabetic monkeys. *Eur Radiol*. 2019;29:3006-3016.
25. Oorschot Joep WM, El AH, Lorkeers SJ, et al. Endogenous assessment of chronic myocardial infarction with T(1ρ)-mapping in patients. *J Cardiovas Magn Resonan*. 2014;16:104.
26. Sebastian B, Joyce H, Mohammed S, Yuchi H, Witschey Walter RT. Measurement of myocardial T1ρ with a motion corrected, parametric mapping sequence in humans. *PLoS One*. 2016;11:e0151144.
27. Van Oorschot Joep WM, Fredy V, Eikendal Anouk LM, et al. Single breath-hold T1ρ-mapping of the heart for endogenous assessment of myocardial fibrosis. *Invest Radiol*. 2016;51:505-512.
28. Haikun Q, Aurelien B, Thomas K, et al. Respiratory motion-compensated high-resolution 3D whole-heart T1ρ mapping. *J Cardiovasc Magn Reson*. 2020;22.
29. Aurélien B, Solenn T, Soumaya S, et al. Endogenous assessment of myocardial injury with single-shot model-based non-rigid motion-corrected T1 rho mapping. *J Cardiovasc Magn Reson*. 2021;23:1-14.
30. Thompson EW, Kamesh IS, Solomon MP, et al. Endogenous T1ρ cardiovascular magnetic resonance in hypertrophic cardiomyopathy. *J Cardiovasc Magn Reson*. 2021;23:1-9.
31. Chunhua W, Jie Z, Jiayu S, et al. Endogenous contrast T1rho cardiac magnetic resonance for myocardial fibrosis in hypertrophic cardiomyopathy patients. *J Cardiol*. 2015;66:520-526. doi:10.1186/s12968-020-0597-5
32. Lin W, Jing Y, Jun ZS, et al. Myocardial T1rho mapping of patients with end-stage renal disease and its comparison with T1 mapping and T2 mapping: a feasibility and reproducibility study. *J Magn Reson Imaging*. 2016;44:723-731.
33. Keyan W, Wenbo Z, Shuman L, et al. Noncontrast T1ρ dispersion imaging is sensitive to diffuse fibrosis: a cardiovascular magnetic resonance study at 3T in hypertrophic cardiomyopathy. *Magn Reson Imaging*. 2022;91:1-8.
34. Witschey Walter RT, Arijitt B, Elliott MA, et al. Artifacts in T1ρ-weighted imaging: compensation for B1 and B0 field imperfections. *J Magn Reson*. 2007;186:75-85.
35. Han Q, Han Y, Gorman RC, Witschey WR. The influence of static and RF field heterogeneity on T1rho cardiovascular MRI. *J Cardiovasc Magn Reson*. 2014;16:1-3.

36. Charagundla SR, Borthakur A, Leigh JS, Reddy R. Artifacts in T1ρ-weighted imaging: correction with a self-compensating spin-locking pulse. *J Magn Reson*. 2003;162:113-121.
37. Maximilian G, Michael S, Daniel G, Johannes O, Jakob PM, Peter N. Balanced spin-lock preparation for B1-insensitive and B0-insensitive quantification of the rotating frame relaxation time T1ρ. *Magn Reson Med*. 2021;85:2771-2780.
38. Michael G, Lance D. The return of the frequency sweep: designing adiabatic pulses for contemporary NMR. *J Magn Reson*. 2001;153:155-177.
39. Peter K, Hansen MS. T1-mapping in the heart: accuracy and precision. *J Cardiovasc Magn Reson*. 2014;16:1-20.
40. Reza N, Matthias S, Ronald O, Gharib AM, Desai MY, Pettigrew RI. B1-insensitive T2 preparation for improved coronary magnetic resonance angiography at 3 T. *Magn Reson Med*. 2006;55:858-864.
41. Shalom M, Sorce DJ, Springer CS, Kamil U, Michael G. T1ρ MRI contrast in the human brain: modulation of the longitudinal rotating frame relaxation shutter-speed during an adiabatic RF pulse. *J Magn Reson*. 2006;181:135-147.
42. Silvia M, Timo L, Michael G, Shalom M. Rotating frame relaxation during adiabatic pulses vs. conventional spin lock: simulations and experimental results at 4 T. *Magn Reson Imaging*. 2009;27:1074-1087.
43. Sorce DJ, Shalom M, Michael G. Relaxation during adiabatic radiofrequency pulses. *Curr Anal Chem*. 2007;3:239-251.
44. Shalom M, Sorce DJ, Michael G. T2ρ and T1ρ adiabatic relaxations and contrasts. *Curr Anal Chem*. 2008;4:8-25.
45. Saeed J, Yajun M, Akhil K, et al. Ultrashort echo time adiabatic T1ρ (UTE-Adiab-T1ρ) is sensitive to human cadaveric knee joint deformation induced by mechanical loading and unloading. *Magn Reson Imaging*. 2021;80:98-105.
46. Tomoyuki O, Yukihisa T, Akihiro N, et al. T1rho mapping improvement using stretched-type adiabatic locking pulses for assessment of human liver function at 3T. *Magn Reson Imaging*. 2017;40:17-23.
47. Levitt MH. Composite pulses. *Prog Nucl Magn Reson Spectrosc*. 1986;18:61-122.
48. Sebastian W, Fabian Z, Metzger GJ, Kâmil U, Van MPF, Mehmet A. Motion-robust cardiac mapping at 3T using interleaved Bloch-Siegert shifts. *Magn Reson Med*. 2017;78:670-677.
49. Noeske R, Seifert F, Rhein K-H, Rinneberg H. Human cardiac imaging at 3T using phased array coils. *Magn Reson Med*. 2000;44:978-982.
50. Schär M, Vonken E-J, Stuber M. Simultaneous B0- and B1+-map acquisition for fast localized shim, frequency, and RF power determination in the heart at 3T. *Magn Reson Med*. 2010;63:419-426.
51. Mehmet A, Basha TA, Sebastian W, Sébastien R, Sophie B, Reza N. Improved quantitative myocardial T2 mapping: impact of the fitting model. *Magn Reson Med*. 2015;74:93-105.
52. Ogg RJ, Kingsley PB, Taylor JS. WET, a T1-and B1-insensitive water-suppression method for in vivo localized 1H. *NMR Spectrosc J Magn Resonan Ser B*. 1994;104:1-10.
53. Captur G, Gatehouse P, Keenan KE, et al. A medical device-grade T1 and ECV phantom for global T1 mapping quality assurance — the T1 mapping and ECV standardization in cardiovascular magnetic resonance (T1MES) Program. *J Cardiovasc Magn Resonan*. 2016;18:1-20.
54. Sebastian W, Desmond KL, Obuchowski NA, et al. Development, validation, qualification, and dissemination of quantitative MR methods: overview and recommendations by the ISMRM quantitative MR study group. *Magn Reson Med*. 2022;87:1184-1206.
55. Isensee F, Jaeger PF, Kohl SAA, Petersen J, Maier-Hein KH. nnU-net: a self-configuring method for deep learning-based biomedical image segmentation. *Nat Methods*. 2020;18:203-211.
56. Zhao Y, Yang C, Schweidtmann A, Tao Q. Efficient Bayesian uncertainty estimation for nnU-net. In: Wang L, Dou Q, Fletcher PT, Speidel S, Li S, eds. *Medical Image Computing and Computer Assisted Intervention – MICCAI 2022. MICCAI 2022*. Lecture Notes in Computer Science. Vol 13438. Springer; 2022.
57. Thomas A, Treibel MF, Maestrini V, et al. Automatic measurement of the myocardial Interstitium: synthetic extracellular volume quantification without Hematocrit sampling. *J Am Coll Cardiol Img*. 2016;9:54-63.
58. Tao Q, van der Tol P, Berendsen FF, et al. Robust motion correction for myocardial T1 and extracellular volume mapping by principle component analysis-based groupwise image registration. *J Magn Reson Imaging*. 2018;47:1397-1405.
59. Nina H, Jari R, Lassi R, Simo S, Nissi MJ. Orientation anisotropy of quantitative MRI relaxation parameters in ordered tissue. *Sci Rep*. 2017;7:1.
60. Eric A, Kévin M, Patrick M, Ennis DB. Quantifying precision in cardiac diffusion tensor imaging with second-order motion-compensated convex optimized diffusion encoding. *Magn Reson Med*. 2018;80:1074-1087.
61. Ferreira VM, Holloway CJ, Piechnik SK, Karamitsos TD, Neubauer S. Is it really fat? Ask a T1-map. *Eur Heart J*. 2013;14:1060.
62. Peter Kellman W, Bandettini P, Mancini C, Hammer-Hansen S, Hansen MS, Arai AE. Characterization of myocardial T1-mapping bias caused by intramyocardial fat in inversion recovery and saturation recovery techniques. *J Cardiovasc Magn Reson*. 2015;17:1-11.
63. Mordi I, Radjenovic A, Stanton T, et al. Prevalence and prognostic significance of lipomatous metaplasia in patients with prior myocardial infarction. *JACC Cardiovasc Imaging*. 2015;8:1111-1112.
64. Kamesh IS, Brianna M, Eileen H, et al. Accelerated free-breathing 3D T1ρ cardiovascular magnetic resonance using multicoil compressed sensing. *J Cardiovasc Magn Reson*. 2019;21:1-11.
65. Carlos V, Gastão C, Begoña L, et al. Simultaneous T1, T2, and T1ρ cardiac magnetic resonance fingerprinting for contrast agent–free myocardial tissue characterization. *Magn Reson Med*. 2022;87:1992-2002.

SUPPORTING INFORMATION

Additional supporting information may be found in the online version of the article at the publisher's website.

Figure S1. Phantom $T_{1\rho,adiab}$ maps acquired with different rest periods for longitudinal magnetization recovery delays. $T_{1\rho,adiab}$ values (± SD) reported in the plot are measured from the normal myocardium-mimicking vial

(left column, middle row). For longitudinal magnetization recovery delays ≥ 3000 ms, the measured $T_{1\rho,adiab}$ values deviate less than 5% from the asymptotic value.

Figure S2. (A) Example of $T_{1\rho,adiab}$ and $T_{1\rho}$ maps of the tissue-mimicking T1MES phantom. Good map quality was achieved with aSL preparations, whereas visible artifacts are apparent in most vials in the maps obtained with RefSL preparation. Approximate T_1 and T_2 maps are displayed for reference. (B) $T_{1\rho,adiab}$ and $T_{1\rho}$ values with SD bars for each vial, averaged over 10 repetitions. $T_{1\rho,adiab}$ values are consistently higher than $T_{1\rho}$ values measured with RefSL preparations. $T_{1\rho,adiab}$ dispersion is observed across B_0, Bal and B_1 optimized pulses, due to a progressively lower β value. (C) Repeatability measured as the coefficient of variability ($\overline{wCV_i}$) for each vial. Averaging across all the vials, aSL preparations yielded significantly improved repeatability ($\overline{wCV_i} = 0.29 \pm 0.15$ for B_0-aSL, $p < 0.01$; $\overline{wCV_i} = 0.23 \pm 0.13$ for Bal-aSL, $p < 0.01$; $\overline{wCV_i} = 0.21 \pm 0.11$ for B_1-aSL, $p < 0.001$ versus $\overline{wCV_i} = 1.30 \pm 1.34$ for RefSL).

Figure S3. $T_{1\rho,adiab}$ maps obtained with B_0-aSL, Bal-aSL and B_1-aSL preparations. Image quality is compromised due to artifacts visible in the maps for B_0-aSL in (A) and for Bal-aSL in (B). Furthermore Bal-aSL prepared baseline images were subject to substantial residual motion in both patients, lowering the image quality.

Table S1. In vivo myocardial $T_{1\rho,adiab}$ values (ms), averaged over all repetitions and segments for six healthy volunteers of cohort 1.

Table S2. In vivo myocardial $T_{1\rho,adiab}$ precision, reproducibility and inter-subject variability (ISV), averaged over segments and repetitions for 6 healthy volunteers of cohort 1.

Table S3. In vivo myocardial $T_{1\rho,adiab}$ and $T_{1\rho}$ values (ms), averaged over all repetitions and segments for seven healthy volunteers of cohort 2.

Table S4. In vivo myocardial $T_{1\rho,adiab}$ and $T_{1\rho}$ precision, reproducibility and inter-subject variability (ISV) averaged over segments and repetitions for seven healthy volunteers of cohort 2.

How to cite this article: Coletti C, Fotaki A, Tourais J, et al. Robust cardiac T_{1_ρ} mapping at 3T using adiabatic spin-lock preparations. *Magn Reson Med*. 2023;1-17. doi: 10.1002/mrm.29713